Perfect dielectric-metamaterial reflector

Brian Slovick,[1,*] Zhi Gang Yu,[1] Marcy Berding,[2] and Srini Krishnamurthy[1]
[1]*SRI International, Applied Optics Laboratory, 333 Ravenswood Avenue, Menlo Park, California 94025, USA*
[2]*SRI International, Materials Research Laboratory, 333 Ravenswood Avenue, Menlo Park, CA 94025, USA*
(Received 19 February 2013; revised manuscript received 24 July 2013; published 9 October 2013)

We exploit the Mie resonance in dielectric microparticles to design a single-negative metamaterial monolayer with near-unity reflectivity and negligible absorptivity. In contrast to Bragg reflectors and photonic band gap materials, which require multiple layers for high reflection, this metamaterial is both highly reflective and subwavelength in thickness. We identify the underlying physics necessary to design near-perfect all-dielectric reflectors at virtually any wavelength band of interest. Using full-wave, finite-element analysis and realistic optical constants for the constitutive materials, we develop a 0.45-μm-thick, silicon-based metamaterial monolayer with normal-incidence reflectivity over 99.999% and absorptivity less than 0.001% at a short-wave infrared wavelength of 1.5 μm.

DOI: 10.1103/PhysRevB.88.165116 PACS number(s): 42.79.Fm, 81.05.Xj, 78.67.Pt, 42.70.Qs

I. INTRODUCTION

The ability to derive a composite medium with optical properties much different from those of the constitutive materials makes metamaterials (MMs) of considerable scientific and technological interest.[1–3] Over the last decade, as the operating frequency of MMs has progressed from GHz and THz to infrared and visible, MMs have enabled the realization of numerous fascinating electromagnetic properties, including a negative refractive index,[4] sub-diffraction-limited imaging,[5] zero reflection by impedance matching,[6] and enhanced optical transmission,[7] reflection, and absorption.[8–10] Most of the initial research at GHz and THz exploited the magnetic-dipole resonance in the split-ring resonator to achieve negative permeability and the electric-dipole resonance in metallic wires to achieve negative permittivity.[11] The extension of these traditional MM design principles to infrared and visible frequencies has been limited primarily by the absorption loss and fabrication complexity associated with the metallic elements.[12]

All-dielectric MMs offer the possibility of achieving properties similar to their metallic counterparts, but with substantially less absorption loss and fabrication complexity.[13] O'Brien and Pendry[14] were the first to exploit Mie resonance to obtain a bulk magnetic polarization from an array of dielectric cylinders. Since then, numerous authors have predicted and measured interesting optical properties in all-dielectric MMs.[13,15–22] Of particular interest is the measured[15,20–22] and predicted[16,18] reflectivity spectra from thin layers of all-dielectric MMs, which show considerably enhanced reflection near the Mie resonance. Although the enhanced reflection was associated with electric and magnetic resonances, its precise physical origin has not been studied in detail. A fundamental physical understanding of the observed reflectance will help to further enhance the performance and perhaps achieve a MM layer with near-perfect reflectivity, which forms the core objective of this article.

A compact, nonabsorbing, perfectly reflecting layer would have numerous important applications. In bio-imaging and nanosensing, a perfect reflector would support a standing wave with a perfect electric-field node at the surface, which could be used to enhance the absorption cross section for circular dichroism in microscopic chiral molecules such as DNA.[23] A perfect reflector could be used to improve the throughput efficiency of lasers by reducing optical loss in the walls of the cavity, and to improve the damage-threshold irradiance of conventional optical devices such as mirrors and filters. While high reflectivity can be obtained with Bragg reflectors and related photonic band gap structures, these often require many layers to achieve the desired reflectivity.[24] An additional advantage of MMs is that they do not necessarily require periodicity if they are truly homogeneous media,[25] and so they offer the possibility of self-assembly growth or paintlike fabrication, making them suitable for large-area applications.

In this article, we first derive the conditions on the permittivity and permeability to achieve perfect reflection for a semi-infinite (bulk) medium. For high-permittivity spheres in air background, we use the Lewin effective medium theory[26] to design a bulk MM with the required effective parameters, and show the corresponding perfect reflectance. Then we derive the additional conditions necessary to achieve perfect reflection for thin layers. As an illustration, we consider a monolayer of Si microspheres in air background. Using measured optical constants for Si, we use finite-element full-wave analysis to design a thin reflector with near-unity reflectance at a short-wave infrared wavelength of 1.5 μm. The high reflectivity is correlated with the calculated permittivity and permeability of the MM monolayer. Finally we design a demonstrable structure of 0.45 μm Si cubes on SiO_2 substrate with over 99.999% reflectivity and less than 0.001% absorptivity at 1.5 μm. The fundamental physical design principles developed here can be used to design a subwavelength-thick, nearly perfect reflector at arbitrary wavelengths of interest.

II. SEMI-INFINITE MEDIUM

First we derive the conditions for perfect reflection for a semi-infinite medium and then obtain additional requirements imposed by finite thickness. The amplitude reflection coefficient r and reflectance R for a semi-infinite medium at normal incidence from vacuum are

$$r = \frac{z-1}{z+1} \tag{1}$$

and

$$R = |r|^2 = \frac{(z'-1)^2 + z''^2}{(z'+1)^2 + z''^2}, \tag{2}$$

where z is the complex impedance, given by $\sqrt{\mu/\epsilon}$, ϵ is the complex permittivity, and μ is the complex permeability. The primes (double primes) denote the real (imaginary) components. We want to identify the conditions on ϵ and μ for perfect reflection, which requires $R = 1$. It can be shown that all solutions require $z' = 0$ with no specific condition on z''. Noting that ϵ and μ are complex numbers, after simple arithmetic manipulations, the solution $z' = 0$ leads to the conditions

$$\frac{\epsilon'}{\mu'} < 0 \tag{3a}$$

and

$$\epsilon''\mu' - \mu''\epsilon' = 0. \tag{3b}$$

The first condition in Eq. (3a) requires that ϵ' and μ' have opposite sign. This clearly means that at the wavelength of interest we need a MM with a resonance either in ϵ or μ, but not both, i.e., a single-negative MM. This is in contrast to negative-index materials which require both ϵ' and μ' to be negative. Although the second condition in Eq. (3b) appears more restrictive, it is satisfied when ϵ and μ are purely real. When the frequency-dependent ϵ' (or μ') changes sign near a resonance, the Kramers-Kronig relationship (KKR) imposed by causality requires that the imaginary part reaches a local maximum. In a medium composed of nonabsorbing constituents, the function ϵ'' (or μ'') will take the form of a δ function, resulting in frequency regions where the conditions in Eq. (3) are fully satisfied. We also note that Eqs. (3a) and (3b) are satisfied mathematically when the imaginary parts of ϵ and μ have opposite sign and their ratio satisfies Eq. (3b). Although this scenario cannot occur in a real passive homogeneous medium,[27] it has been predicted[28] and measured[29] in inhomogeneous periodic metamaterials.

While Eqs. (3a) and (3b) are useful from a conceptual point of view, for realistic materials with absorption Eq. (3b) is not satisfied and $z' \neq 0$. In this case, it follows from Eq. (2) that the reflectivity is greater than $1 - \delta$ for any positive $\delta \leqslant 1$ if z is outside the circle

$$\left| z - \left(\frac{2}{\delta} - 1 \right) \right|^2 > \left(\frac{2}{\delta} - 1 \right)^2 - 1 \tag{4}$$

in the $z' > 0$ half plane. So it is clear that arbitrarily high reflectivity can be achieved for z' sufficiently close to zero. After further algebraic analysis, it can be shown that the right-hand side of Eq. (3b) is of the order of δ, indicating that the maximum reflectivity is obtained when the left-hand side of Eq. (3b) is minimized.

To explore this solution further, we consider a MM based on the Mie resonance in dielectric spheres. Mie resonances originate from the scattering of electromagnetic fields in a high-permittivity sphere surrounded by a low-permittivity background.[30] The lowest-energy resonance is a magnetic dipole and it occurs when the wavelength in the sphere is comparable to the diameter. For a single isolated sphere with real permittivity ϵ_s, real permeability μ_s, and diameter d, the magnetic-dipole resonance occurs for the approximate free-space wavelength

$$\lambda_0^{\text{res}} = d\sqrt{\epsilon_s \mu_s}, \tag{5}$$

independent of the background permittivity ϵ_b for large dielectric contrast.[30–32] Near the magnetic-dipole resonant frequency, a composite medium of identical spheres can acquire an effective bulk magnetic polarization, which can result in a negative effective permeability ($\mu' < 0$) with ϵ real and positive ($\epsilon' > 0$).[31,32] Similarly, near the electric-dipole resonant frequency, the effective ϵ' can be negative when μ' is positive. Under these conditions, the requirements for perfect reflection in Eq. (3) can be met.

For illustration, first we consider a semi-infinite dilute medium of nonmagnetic ($\mu_s = 1$) dielectric spheres with large permittivity ($\epsilon_s = 50$), arranged in a simple-cubic lattice in air background ($\epsilon_b = 1$). To obtain the effective ϵ and μ for the composite, we use the Lewin effective-medium model,[26] which is valid for large dielectric contrast and dilute loading. Using Eq. (5), we choose a particle diameter $d = 0.24$ μm to position the single-particle magnetic-dipole resonance at a free-space wavelength of 1.7 μm. The periodicity is taken as 0.36 μm, which corresponds to a volume-loading density of 15%. We used effective ϵ and μ from the Lewin model in Eq. (2) to calculate the reflectance from vacuum at normal incidence for a semi-infinite medium of the MM. The calculated μ, ϵ, and R are shown in Fig. 1. As shown in Fig. 1(a), the effective μ' has a resonance around 1.74 μm, in good agreement with the single-particle resonance condition. We also see that $\mu' < 0$ for wavelengths between 1.6 and 1.74 μm, with μ'' nearly equal to zero in that band, except very close to the resonance. Similarly, an electric-dipole resonance occurs at 1.2 μm [Fig. 1(b)], but with a much narrower band exhibiting $\epsilon' < 0$ and $\epsilon'' \approx 0$. The shaded regions in Figs. 1(a) and 1(b) show the bands where Eq. (3) is fully satisfied. As shown in Fig. 1(c), the calculated reflectivity in these regions is near unity as expected. If more absorptive constitutive materials are used, the functional form of μ'' and ϵ'' becomes a Lorentzian with finite width, and the bandwidth and amplitude of the high-reflection regions are reduced.

III. THIN LAYER

For realistic MMs with finite layer thickness, additional conditions for perfect reflection must be satisfied. The amplitude reflection coefficient S_{11} at normal incidence for a MM layer of thickness t and complex refractive index n in vacuum is given by[33]

$$S_{11} = \frac{r[1 - \exp(j2k_0nt)]}{1 - r^2 \exp(j2k_0nt)}, \tag{6}$$

where r is given by Eq. (1) and $k_0 = 2\pi/\lambda_0$. As before, for perfect reflection, R (which is now $|S_{11}|^2$) $= 1$. Then the exact solution is $z = 0$, which is quite restrictive because it requires that both ϵ and μ are zero. If instead $z \neq 0$ but $z' = 0$, near-perfect reflection is still possible, depending on the value of n''. Substituting Eq. (1) with $z' = 0$ into Eq. (6), we obtain

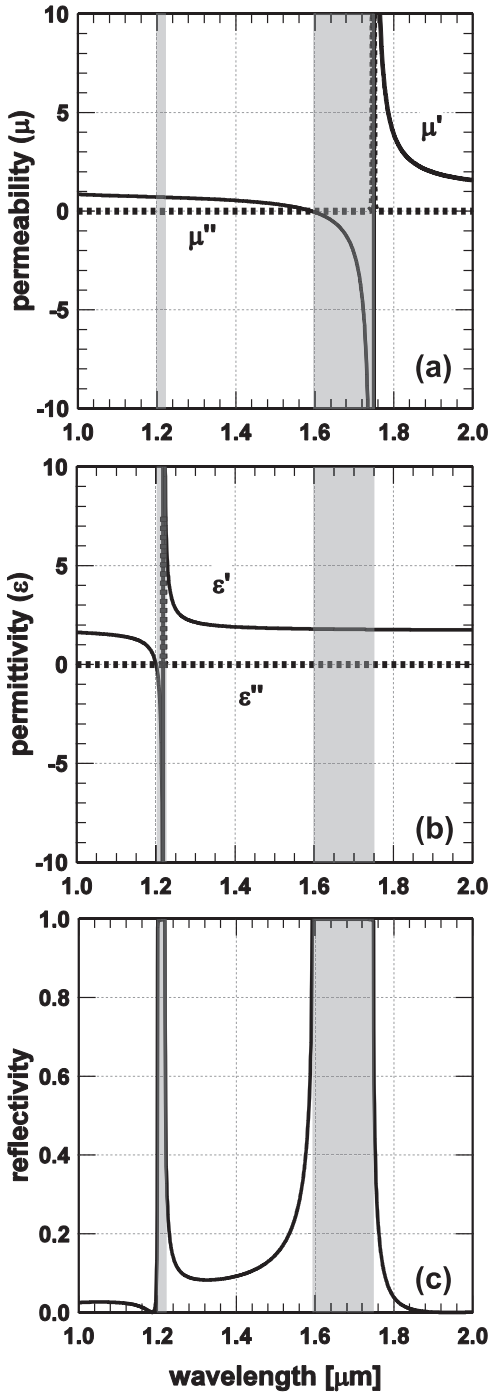

FIG. 1. (a) Permeability, (b) permittivity, and (c) reflectivity for a semi-infinite medium of dielectric spheres with $\epsilon_s = 50$, arranged in a simple-cubic lattice, calculated using the Lewin effective-medium model. The solid (dotted) lines show the real (imaginary) parts and the shaded regions show the bands where the conditions for perfect reflection in Eq. (3) are fully satisfied.

the following condition on n'' to achieve a reflectance of $R = 1 - \delta$:

$$n'' = \frac{\lambda_0}{4\pi t} \ln\left(\frac{4}{\delta}\right). \tag{7}$$

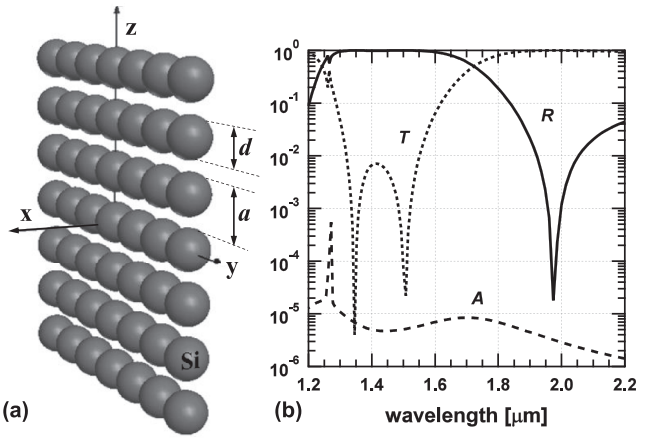

FIG. 2. (a) Schematic of the monolayer of Si microspheres and (b) calculated reflectance R, transmittance T, and absorbance A for normal-incident light from vacuum.

For a thin layer, t is small and the required n'' is large. Further, since n is given by $\sqrt{\epsilon\mu}$, we obtain

$$n'' = \sqrt{|\epsilon||\mu|}\,\sin\left[\frac{1}{2}\tan^{-1}\left(\frac{\epsilon''\mu' + \epsilon'\mu''}{\epsilon'\mu' - \epsilon''\mu''}\right)\right]. \tag{8a}$$

Hence, n'' is maximized when the product $|\epsilon||\mu|$ is large and

$$\epsilon'\mu' = \epsilon''\mu''. \tag{8b}$$

For illustration, we apply these guidelines to obtain high reflectivity using a monolayer of silicon microspheres. Although the generic optical properties of Si spheres and Si-sphere arrays were studied previously,[19,34,35] such structures have not been designed specifically to achieve high reflectivity. Our MM structure consists of a monolayer of Si spheres of diameter d in vacuum ($\epsilon_b = 1$), arranged in a square lattice with center-to-center spacing a, as shown in Fig. 2(a). The light propagation is along the **x** direction. In the current structure, the periodicity is chosen to be comparable to the particle diameter, so the Lewin and other analytical models are not expected to yield accurate values for the effective ϵ and μ. Instead we solve the Maxwell equations numerically using the commercial finite-element solver HFSS (Ansys), whose accuracy has been verified previously.[25] In the calculations, we use measured data for the frequency-dependent permittivity of Si,[36] which in the 1–2 μm band is nearly constant with a value around $\epsilon_s = 12 + j10^{-5}$. From Eq. (5), the particle size d required to position the single-particle magnetic resonance at 1.5 μm is 0.43 μm. Although this simple resonance condition is strictly valid for a single isolated sphere, it serves as a convenient initial guess for the full-wave analysis. Starting with this value, we vary d and a in HFSS to achieve $|S_{11}|^2 \to 1$ near $\lambda_0 = 1.5$ μm. The final optimized structure has $a = 0.63$ μm and $d = 0.5$ μm, corresponding to a volume loading density of 26%.

The HFSS calculations of reflectance R, transmittance T, and absorbance A for normal incidence and a single layer of this material are shown in Fig. 2(b). Near $\lambda_0 = 1.5$ μm the reflectance reaches a maximum of 99.997% with absorptivity less than 10^{-5}. The predicted reflectance is larger than 99% for

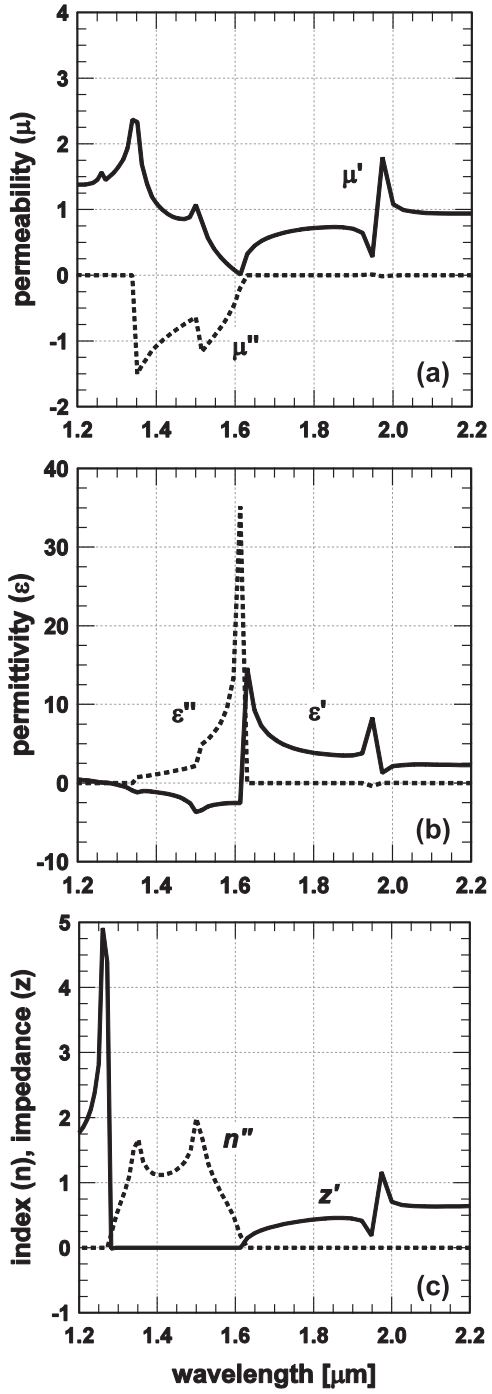

FIG. 3. (a) Permeability, (b) permittivity, and (c) imaginary refractive index and real impedance for the monolayer of Si microspheres in Fig. 2(a), calculated from the transmission/reflection coefficients determined in HFSS. We note that the region where $z' = 0$ and $n'' \gg 0$ in (c) coincides with the high-reflectivity band in Fig. 2(b).

wavelengths between 1.3 and 1.55 μm. Using the previously documented procedure,[25,33,37] the effective parameters μ, ϵ, n, and z are calculated from the transmission and reflection coefficients for a single layer of the MM. Although z and n'' are determined unambiguously by this procedure, there are an infinite number of solutions for n'. The correct value for n' is identified as the solution with the smallest difference from that calculated using the KKR.[38] We further verified that the calculated effective parameters at long wavelengths are consistent with those deduced from Maxwell-Garnett effective-medium theory.

The calculated μ and ϵ are shown in Figs. 3(a) and 3(b), respectively, and Fig. 3(c) shows the effective z' and n''. As the wavelength decreases from 2.2 μm, the effective μ' [Fig. 3(a)] increases toward the first Mie resonance, which occurs at 1.95 μm. For the chosen particle diameter of 0.5 μm, the single-particle Mie resonance would be at $\lambda_0^{\text{res}} = 1.73$ μm, so the effective resonance in the monolayer is redshifted relative to the single-particle resonance. This redshift originates from diffraction-coupling between the resonant spheres.[19] There is a corresponding antiresonance in the effective ϵ [Fig. 3(b)] due to the effects of spatial dispersion.[27,28] The magnitude of the magnetic-dipole resonance is relatively small and does not result in a negative value for μ'. Consequently, the reflectance in Fig. 2(b) at 1.95 μm is low. Just below 2 μm, where the impedance of the monolayer is matched to free space ($z' = 1$), the reflectivity reaches a local minimum. A similar result was obtained with Si-particle monolayers in the visible band.[19] As the wavelength decreases below 1.9 μm, the effective ϵ' increases until the onset of the electric-dipole resonance at $\lambda_0 = 1.6$ μm. For wavelengths between 1.6 μm and 1.25 μm, $\epsilon' < 0$ and $\mu' > 0$ [Figs. 3(a) and 3(b)], thus meeting the first requirement for perfect reflection in Eq. (3a). We also find in the same band that the effective z' [solid line in Fig. 3(c)] is close to zero, implying that the additional constraint in Eq. (3b) is satisfied. We further note that the constraint imposed by finite thickness in Eq. (7) is also satisfied throughout most of this band, and the maximum values of n'', which by Eqs. (3b) and (8b) coincide with the regions where $|\mu'| = |\mu''|$ and $|\epsilon'| = |\epsilon''|$, correlate precisely with the reflection maxima, or equivalently transmission minima, in Fig. 2(b).

To verify that the resonances in ϵ and μ in Fig. 3 correspond to single-particle Mie resonances, we show in Fig. 4 the electric and magnetic field vectors in the unit cell of the MM, for wavelengths close to the resonances in Fig. 3. The electric **E** (magnetic **H**) field is shown in the $y = 0$ ($z = 0$) plane and the incident electric field is polarized along the **z** axis. At a wavelength of 1.95 μm, where a small resonance in μ is apparent in Fig. 3(a), there is a maximum in the magnetic field vector at the center of the sphere and a corresponding ring-shaped displacement electric field vector. These are distinct characteristics of the magnetic-dipole mode.[20,30,35] Similarly, at 1.67 μm, near the onset of the high-reflectivity band and the resonance in ϵ, the electric-field vector clearly resembles an electric dipole with a surrounding induced circular displacement magnetic field. We further note (not shown) that for a wavelength of 1.25 μm, where in Fig. 3(a) there is a small additional peak in μ', there are two maxima in the magnetic-field vector in the sphere, indicating the presence of the magnetic-quadrupole mode.

For the MM described above, near-perfect reflectance is possible with only a single layer of material because the origin of reflectivity is a single-scatterer Mie resonance within the unit cell rather than multiple Bragg scattering between cells. While both scattering mechanisms are present in some photonic crystals,[14,24] the band gaps of interest usually

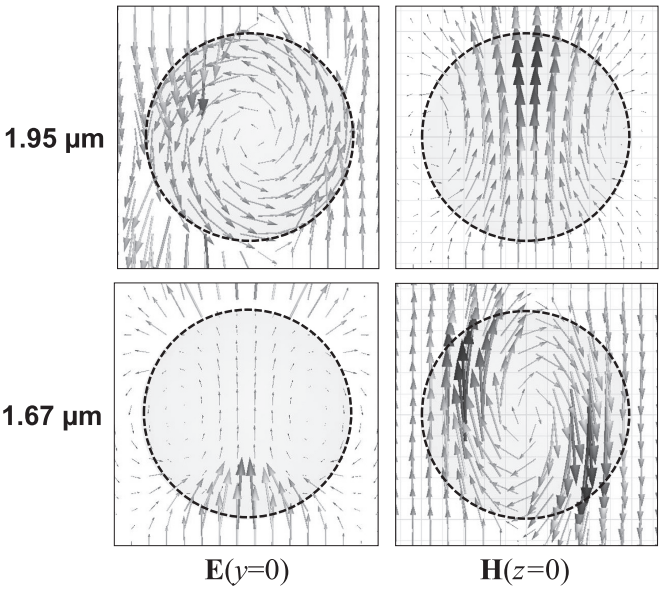

FIG. 4. Electric **E** (magnetic **H**) field vector in the $y = 0$ ($z = 0$) plane of the unit cell of the MM in Fig. 2(a), for wavelengths near the resonances in μ and ϵ in Fig. 3. The incident electric field is polarized along the **z** axis and propagation is from left to right along the **x** axis.

originate from Bragg scattering, so more layers are required to achieve reflection comparable to our MM design. For example, we find that the reflectivity at $\lambda_0 = 1.5$ μm is 100% as predicted[39] in the band gap of a photonic crystal of lossless Si spheres ($d = 0.42$ μm) in the diamond-lattice structure. However, the reflectivity from a single layer (1.2 μm thick) of this material is only 80% at normal incidence. Similarly, very high reflectivity can be obtained using a planar quarter-wave stack of alternating constitutive materials. However we find that the reflection from a 0.58-μm-thick stack (of three layers) is only 97% at normal incidence. The thickness must be increased at least three times to achieve the performance predicted for our MM monolayer.

IV. NEAR-PERFECT THIN REFLECTOR: DEMONSTRABLE DESIGN

For possible fabrication and verification, we now consider a demonstrable design of Si microcubes on SiO_2 substrate ($\epsilon = 2.1 + j10^{-5}$). A schematic of the structure is shown in Fig. 5(a). Although similar structures were studied previously,[15,20,21] our MM is optimized specifically to achieve high reflectivity. Similarly to dielectric spheres, cubes also support Mie-like resonances. However, cubes can be readily fabricated using lithography.[15] As with previous designs, the MM parameters are chosen to achieve $|S_{11}|^2 \to 1$ near $\lambda_0 = 1.5$ μm with an initial value of $d = 0.43$ μm, given by the Mie-resonance condition for cubes, which is equivalent to Eq. (5) with the diameter replaced by the cube length.[40] This optimization resulted in $d = 0.45$ μm and $a = 0.67$ μm. The calculated reflectance, transmittance, and absorbance for propagation normal to the monolayer are shown in Fig. 5(b). Near 1.5 μm, the reflectivity reaches a maximum of 99.999% (as evidenced by the transmission minimum) with less than

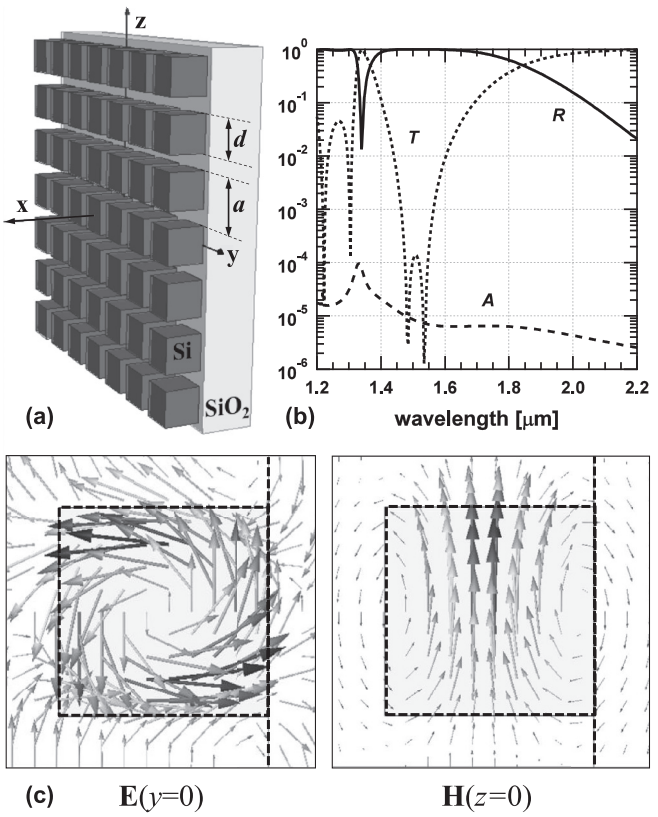

FIG. 5. (a) Schematic of the monolayer of Si microcubes, (b) the calculated reflectance R, transmittance T, and absorbance A for normal-incident light from vacuum, and (c) the electric **E** (magnetic **H**) field vector in the $y = 0$ ($z = 0$) plane of the unit cell of the MM for a wavelength of 1.6 μm. The incident electric field is polarized along the **z** axis and propagation is from left to right along the **x** axis.

10^{-5} absorptivity. The electromagnetic fields at 1.6 μm, shown in Fig. 5(c), clearly resemble a magnetic-dipole mode, thus confirming that the onset of the high-reflectivity band for the cube structure is also near a single-particle Mie resonance.

As the angle of incidence increases away from normal, the reflectivity (not shown) gradually decreases to 90% at 20° and 40% at 50°, before increasing back to total reflection at grazing angles. We emphasize that the structure described here is not specifically optimized for high reflectivity over broad angles, as the conditions for perfect reflection [Eqs. (3a), (3b), and (7)] were obtained for normal incidence. We also note that the reflectivity off normal can be improved with additional layers, and that work is currently in progress to fabricate this structure and measure its wavelength- and angle-dependent reflection and absorption properties.

V. CONCLUDING REMARKS

In several previous publications, both theory and measurements, high reflectivity was observed in thin layers of dielectric-metamaterial structures.[15,16,21] In these studies,

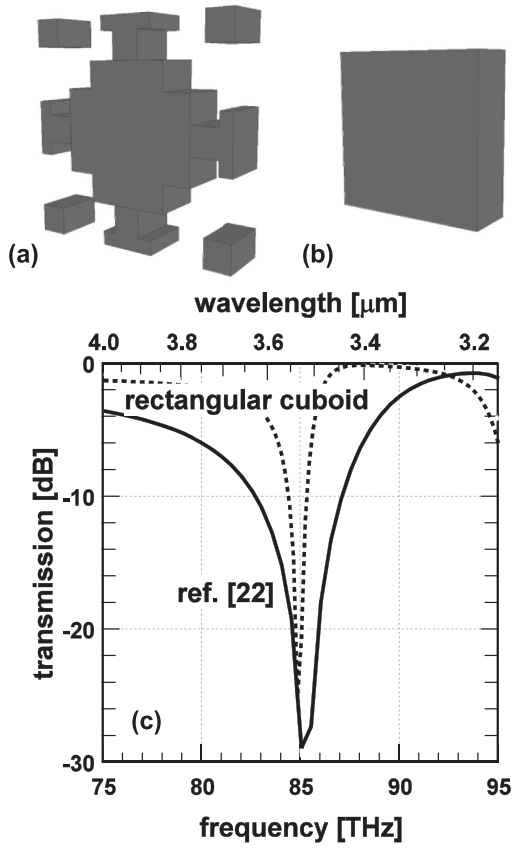

FIG. 6. Unit cell of metamaterial structure (a) from Ref. 22 and (b) of a rectangular cuboid with the same thickness, and (c) the calculated (solid) transmission measured in Ref. 22 and predicted (dotted) transmission for the structure in (b).

although not stated explicitly, the enhanced reflection occurs when either μ' or ϵ' is negative, z' is near zero, and n'' is large, as described in this article. Recently, Namin *et al.*[22] using a genetic algorithm designed a detailed subwavelength-thick MM structure of a-Si on SiO_2 substrate, whose unit cell is shown Fig. 6(a), and demonstrated high reflectance (low transmittance) at 85 THz as shown in Fig. 6(c). Without changing the material properties, unit-cell length (2.05 μm), and layer thickness (of 0.47 μm), we modified the original structure in Fig. 6(a), to a rectangular cuboid of side length 1.45 μm, as shown in Fig. 6(b). We note the similarity between this structure and our Mie-resonance-based MM design in Fig. 5(a). The calculated frequency-dependent transmission for structure (b), shown in Fig. 6(c), is remarkably similar to that of structure (a), suggesting that the origin of high-reflectivity in the detailed structure from Ref. 22 is also a Mie-like resonance. These results suggest that a fundamental physics-based approach using Mie resonance in various dielectric particles can be used to design subwavelength-thick, all-dielectric metamaterials with high reflectivity and negligible absorptivity.

In summary, we developed a procedure to exploit the Mie resonance in dielectric microparticles to design a single-negative metamaterial monolayer with near-unity reflectance and negligible absorbance. We identified the conditions and fundamental physical principles necessary to develop a nearly perfect thin reflector at arbitrary wavelengths of interest. Because the origin of high reflectivity is a single-particle Mie resonance and induced negative permittivity rather than Bragg scattering, only a single layer is required. Using finite-element analysis and realistic materials properties, we designed a subwavelength-thick, Si-based MM layer with normal-incidence reflectivity over 99.999% and absorptivity less than 0.001% at a short-wave infrared wavelength of 1.5 μm.

ACKNOWLEDGMENTS

This work was funded in part by SRI's IR&D program and by ONR (Program Manager, Dr. Mark Spector) through Grant No. N00014-12-1-0722.

*brian.slovick@sri.com

[1]C. M. Soukoulis and M. Wegener, Nat. Photonics **5**, 523 (2011).
[2]Y. Liu and X. Zhang, Chem. Soc. Rev. **40**, 2494 (2011).
[3]N. I. Zheludev and Y. S. Kivshar, Nat. Mater. **11**, 917 (2012).
[4]D. R. Smith, J. B. Pendry, and M. C. K. Wiltshire, Science **305**, 788 (2004).
[5]A. Grbic and G. V. Eleftheriades, Phys. Rev. Lett. **92**, 117403 (2004).
[6]S. Gu, J. P. Barrett, T. H. Hand, B.-I. Popa, and S. A. Cummer, J. Appl. Phys. **108**, 064913 (2010).
[7]W. Fan, S. Zhang, B. Minhas, K. J. Malloy, and S. R. J. Brueck, Phys. Rev. Lett. **94**, 033902 (2005).
[8]S. O'Brien, D. McPeake, S. A. Ramakrishna, and J. B. Pendry, Phys. Rev. B **69**, 241101 (2004).
[9]N. I. Landy, S. Sajuyigbe, J. J. Mock, D. R. Smith, and W. J. Padilla, Phys. Rev. Lett. **100**, 207402 (2008).
[10]L. Huang and H. Chen, Prog. Electromagn. Res. **113**, 103 (2011).
[11]D. R. Smith, W. J. Padilla, D. C. Vier, S. C. Nemat-Nasser, and S. Schultz, Phys. Rev. Lett. **84**, 4184 (2000).
[12]S. Xiao, V. P. Drachev, A. V. Kildishev, X. Ni, U. K. Chettiar, H. K. Yuan, and V. M. Shalaev, Nature (London) **466**, 735 (2010).
[13]Q. Zhao, J. Zhou, and D. Lippens, Mater. Today **12**, 60 (2009).
[14]S. O'Brien and J. B. Pendry, J. Phys.: Condens. Matter **14**, 6383 (2002).
[15]J. C. Ginn, I. Brener, D. W. Peters, J. R. Wendt, J. O. Stevens, P. F. Hines, L. I. Basilio, L. K. Warne, J. F. Ihlefeld, P. G. Clem, and M. B. Sinclair, Phys. Rev. Lett. **108**, 097402 (2012).
[16]A. Ahmadi and H. Mosallaei, Phys. Rev. B **77**, 045104 (2008).
[17]C. L. Holloway, E. F. Kuester, J. Baker-Jarvis, and P. Kabos, IEEE Trans. Antennas Propag. **51**, 2596 (2003).
[18]I. B. Vendik, M. A. Odit, and D. S. Kozlov, Metamaterials **3**, 140 (2009).
[19]A. B. Evlyukhin, C. Reinhardt, A. Seidel, B. S. Lukyanchuk, and B. N. Chichkov, Phys. Rev. B **82**, 045404 (2010).

[20]Q. Zhao, L. Kang, B. Du, H. Zhao, Q. Xie, X. Huang, B. Li, J. Zhou, and L. Li, Phys. Rev. Lett. **101**, 027402 (2008).

[21]K. Shibuya, K. Takano, N. Matsumoto, K. Izumi, H. Miyazaki, Y. Jimba, and M. Hangyo, in *2nd International Congress on Advanced Electromagnatic Materials in Microwaves and Optics, Pamplona, Spain, 21–26 September 2008* (Metamorphose Virtual Institute, Belgium, 2008), pp. 777–779.

[22]F. Namin, S. Yun, T. S. Mayer, D. H. Werner, and C. Rivero-Baleine, in *IEEE International Symposium on Antennas and Propagation (APSURSI) 2011, Spokane, WA, 3–8 July 2011* (IEEE, Piscataway, 2011), pp. 1155–1158.

[23]Y. Tang and A. E. Cohen, Phys. Rev. Lett. **104**, 163901 (2010).

[24]E. Yablonovitch, J. Opt. Soc. Am. B **10**, 283 (1993).

[25]D. R. Smith, D. C. Vier, T. Koschny, and C. M. Soukoulis, Phys. Rev. E **71**, 036617 (2005).

[26]L. Lewin, J. Inst. Elec. Eng. Part III: Rad. Comm. Eng. **94**, 65 (1947).

[27]L. D. Landau and E. M. Lifshitz, *Electrodynamics of Continuous Media*, 2nd ed. (Butterworth-Heinemann, Oxford, 1984).

[28]T. Koschny, P. Markos, D. R. Smith, and C. M. Soukoulis, Phys. Rev. E **68**, 065602 (2003).

[29]A. F. Starr, P. Rye, D. R. Smith, and S. N. Nemat-Nasser, Phys. Rev. B **70**, 113102 (2004).

[30]C. F. Bohren and D. R. Huffman, *Absorption and Scattering of Light by Small Particles* (John Wiley & Sons Inc., Somerset, NJ, 1983).

[31]M. S. Wheeler, J. S. Aitchison, and M. Mojahedi, Phys. Rev. B **72**, 193103 (2005).

[32]M. S. Wheeler, J. S. Aitchison, and M. Mojahedi, Phys. Rev. B **73**, 045105 (2006).

[33]X. Chen, T. M. Grzegorczyk, B. I. Wu, J. Pacheco, and J. A. Kong, Phys. Rev. E **70**, 016608 (2004).

[34]A. Garcia-Etxarri, R. Gomez-Medina, L. S. Froufe-Perez, C. Lopez, L. Chantada, F. Scheffold, J. Aizpurua, M. Nieto-Vesperinas, and J. J. Saenz, Opt. Express **19**, 4815 (2011).

[35]L. Shi, T. U. Tuzer, R. Fenollosa, and F. Meseguer, Adv. Mater. **24**, 5934 (2012).

[36]E. D. Palik, *Handbook of Optical Constants of Solids I* (Academic Press, San Diego, CA, 1998).

[37]D. R. Smith, S. Schultz, P. Markos, and C. M. Soukoulis, Phys. Rev. B **65**, 195104 (2002).

[38]Z. Szabo, G.-H. Park, R. Hedge, and E.-P. Li, IEEE Microw. Theory **58**, 2646 (2010).

[39]K. M. Ho, C. T. Chan, and C. M. Soukoulis, Phys. Rev. Lett. **65**, 3152 (1990).

[40]J. C. Ginn, G. A. T. Eyck, I. Brener, D. W. Peters, and M. B. Sinclair, in *Photonic Metamaterials and Plasmonics* (Optical Society of America, Tucson, AZ, 2010).